Nano Energy xxx (xxxx) xxx

Contents lists available at ScienceDirect

Nano Energy

journal homepage: http://www.elsevier.com/locate/nanoen

Full paper

Dual-polarity response in self-powered ZnO NWs/Sb_2Se_3 film heterojunction photodetector array for optical communication

Bangsen Ouyang [a,b], Huiqi Zhao [a,b], Zhong Lin Wang [a,b,c,**], Ya Yang [a,b,d,*]

[a] CAS Center for Excellence in Nanoscience, Beijing Key Laboratory of Micro-nano Energy and Sensor, Beijing Institute of Nanoenergy and Nanosystems, Chinese Academy of Sciences, Beijing, 100083, PR China
[b] School of Nanoscience and Technology, University of Chinese Academy of Sciences, Beijing, 100049, PR China
[c] School of Material Science and Engineering, Georgia Institute of Technology, Atlanta, GA, 30332-0245, USA
[d] Center on Nanoenergy Research, School of Physical Science and Technology, Guangxi University, Nanning, 530004, PR China

ARTICLE INFO

Keywords:
Photodetector
Dual-polarity
Self-powered
ZnO
Sb_2Se_3

ABSTRACT

Self-powered photodetectors (PD) have great potential applications in visible light communication (VLC) systems due to their unique advantages such as energy saving and low cost, where color shift keying (CSK) is widely utilized to meet the requirements of non-negative light intensity modulation. However, at least two PDs with filters are needed to decode the optical signals, greatly increasing the device cost and complicating the communication system. Here, we report a new type of dual-polarity response PD with an adjustable polarity switching wavelength, where the output signals are positive and negative in long and short wavelength regions, respectively. The dual-polarity response is a consequence of the competition between photovoltaic (PV) effect of ZnO NWs/Sb_2Se_3 film p-n junction and pohtothermoelectric (PTE) effect of Sb_2Se_3 thin film. As compared with current PDs in CSK systems, our PD can work without any filter and one PD can realize the function of two traditional PDs. This new PDs have the potential applications in optical communication systems and filterless color discrimination.

1. Introduction

Ultraviolet (UV) Self-powered photodetectors (PDs) have attracted broad attention due to its wide-range application scenarios such as communication, imaging and environmental monitoring [1–4]. Current researches on self-powered PD mainly focus on improving the responsivity [3,5,6], response speed [7,8], detectivity [9,10] and fabricating wearable device [11–13]. However, with the development of technology, those traditional PDs may not satisfy the request of some special application scenarios because of the simple detection function. For instance, the development of solid-state lighting has given rise to visible light communication (VLC), where light from LEDs can be both used for illumination and data transmission [14–16]. In VLC systems, color shift keying (CSK) was widely used as the modulation scheme to address the issues such as low data rate, limited dimming support and non-negative optical intensity [14,17]. In CSK modulation systems, signals are modulated on light through LEDs with different color wavelength. Thus, at least two PDs with filters are needed to decode the signals from different LEDs, which greatly add cost to the fabrication of PD and complicate the communication system [17–19]. Besides, those receivers such as camera sensors can only provide very low data rate [14]. Thus, it is of great significance to design new type of PDs with special functions.

Photovoltaic (PV) and Photothermoelectric (PTE) effect are two dominant mechanisms to design self-powered PDs [3,6,7,20–23]. Generally, PV-type self-powered PDs are mainly based on p-n junction, where the built-in electric field near the interface of p-n junction serves as the driving force of the photocurrent [24,25]. Thus, it is of great importance for the PV-type PDs that the incident photons can reach the depletion region near the interface of p-n junction. For PTE-type self-powered PDs, the output current signals depend on the Seebeck coefficient of the materials and the temperature gradient across the device induced by the incident light [26,27]. Hence, illumination region should

* Corresponding author. CAS Center for Excellence in Nanoscience, Beijing Key Laboratory of Micro-nano Energy and Sensor, Beijing Institute of Nanoenergy and Nanosystems, Chinese Academy of Sciences, Beijing, 100083, PR China.
** Corresponding author. CAS Center for Excellence in Nanoscience, Beijing Key Laboratory of Micro-nano Energy and Sensor, Beijing Institute of Nanoenergy and Nanosystems, Chinese Academy of Sciences, Beijing, 100083, PR China.
E-mail addresses: zhong.wang@mse.gatech.edu (Z.L. Wang), yayang@binn.cas.cn (Y. Yang).

https://doi.org/10.1016/j.nanoen.2019.104312
Received 9 October 2019; Received in revised form 11 November 2019; Accepted 17 November 2019
Available online 20 November 2019
2211-2855/© 2019 Elsevier Ltd. All rights reserved.

be controlled to establish a temperature gradient across the device; laser with a small spot size (about hundreds of nanometers) was usually used as the light source to realize a local illumination of the nano device with an effective length about several microns [23,26–28]. Antimony selenide (Sb_2Se_3) have been proven to be an excellent optoelectronic material due its larger absorption coefficient and excellent carrier mobility [29–31]. Besides, the thermoelectric properties of Sb_2Se_3 is also attractive for its large Seebeck coefficient [32–34]. In addition, due to its large absorption coefficient, energy from short wavelength light illumination will be constrained in a small region (as low as dozens of nanometers in thickness); thus, a temperature gradient can be established in Sb_2Se_3 thin film (about 500 nm in thickness). By adopting Sb_2Se_3 as the p-type absorber material of a p-n junction, we can integrate PV and PTE effects in one device and finally acquire a multifunction PD.

Here we present a new type of dual-polarity response self-powered PD based on ZnO NWs/Sb_2Se_3 film heterojunction, where the polarity of the output signal is determined by the wavelength of the incident light. As the wavelength of the incident light increases from 405 nm to 880 nm, the output current gradually switches from negative to positive. The dual-polarity response is a consequence of the competition between PV effect of ZnO NWs/Sb_2Se_3 p-n junction and PTE effect of Sb_2Se_3 thin film. Moreover, the PD was successfully used as a receiver in a bipolar CSK system and the application of photodetector array (4 × 4) shows potential in accurate indoor positioning [16]. As compared with current receivers in CSK systems, our receiver can work without any filter and one receiver can realize the function of two traditional receivers [17]. This new type of PD can reduce the costs of device fabrication and simply the communication system, which shows a great application potential in VLC system. Besides, it can also be used for filterless color discrimination [2,35].

2. Experimental section

2.1. Device fabrication

The commercial ITO glass substrates (<7 Ω/sq) were ultrasonically cleaned by glass lotion, deionized water and ethanol. Then, a layer of Sb_2Se_3 film was deposited on the dried substrates by radio frequency (RF) magnetron sputtering (Ar, 100 W, 2700 s) at room temperature. To obtain p-type Sb_2Se_3, the as-deposited thin films were annealed at 300 °C for 1 h in a horizontal quartz tube furnace under N_2 atmosphere [38]. Subsequently, the ZnO seeds layer was deposited on the surface of Sb_2Se_3 films by RF magnetron sputtering (Ar, 100 W, 3600 s) at room temperature. The seeded substrates were immersed into the mixed nutrient solutions (100 mM $ZnO \cdot 6H_2O$ and 100 mM HMTA) face down for the growth of ZnO NWs via hydrothermal method at 85 °C for 4 h. Afterwards, the ZnO NWs was rinsed with deionized water and dried in a mechanical convection oven. To get photodetector array, double layer Kapton tapes with 16 square holes (4 × 4 array) were struck to the surface of ZnO NWs as masks. A thin layer of silver (Ag) was deposited on the surface of ZnO NWs by direct current magnetron sputtering (Ar, 100 W, 300 s). After the top layer of Kapton tapes were peeled off, the left Kapton tapes were used to glue the copper wires and improve the robustness of the devices.

2.2. Characterization and measurements

The thickness of the device and the morphologies of the Sb_2Se_3 thin film (ZnO NWs) were characterized by field emission scanning electron microscopy (SU8020, Hitachi). A commercial atomic force microscope (ICON, Bruker) was used to acquire the topography of the Sb_2Se_3 film and ZnO NWs. The crystal crystallographic structure of ZnO NWs was obtained by X-ray diffraction with Cu Kα radiation (X'Pert3 Powder, PANalytical). Transmission spectra were measured by UV-VIS-NIR spectrophotometer (UV-3600, SHIMADZU).

A system source meter (2611B, Keithely) in conjunction with a computer was used to recorded the electrical signals. An optical chopper (SR540, Stanford) was used to periodically cut off the light source. The temperature information was obtained by an IR thermographic camera (PI400, Optris). The light intensity was acquired by a laser power meter (Nova II, OPHIR) equipped with a thermal sensor (3A-ROHS, OPHIR).

3. Results and discussion

Fig. 1a illustrates the schematic structure diagram of the self-powered ZnO NWs/Sb_2Se_3 film heterojunction photodetector (PD) array and the light direction. As shown in Fig. 1a, a transparent indium tin oxide (ITO) glass is used as the bottom electrode and substrate, a layer of p-type Sb_2Se_3 thin film works as the absorber material, a layer of n-type ZnO serves as the buffer layer, a layer of Kapton tape is used as the insulation layer, and a thin layer of silver (Ag) works as the top electrode. It is worth noticing that, different from traditional designation, the absorber layer works as the window layer. An optical image of the fabricated photodetector array is demonstrated in Fig. 1b, in which the dimension of the substrate is 2 cm × 2 cm and the active area of each pixel is 3 mm × 3 mm. The device structure is confirmed by the cross-sectional scanning electron microscopy (SEM) image illustrated in Fig. 1c and the effective thickness of the device is approximately 3 μm. As depicted in Fig. 1d, the top-view SEM image of the annealed Sb_2Se_3 thin film indicates that Sb_2Se_3 with large size in grains and compactly grown on the ITO substrate. The inset in Fig. 1d is a topography of the annealed Sb_2Se_3 thin film, which illustrates that the surface of the Sb_2Se_3 thin film is ultra-flat with a root-mean-square roughness (R_q) of 13.2 nm; the flat surface is crucial to the growth of uniform ZnO NWs. As demonstrated in Fig. 1e, the top-view SEM image of the as-grown ZnO NWs illustrates that the ZnO NWs are uniformly and densely grown on the surface of Sb_2Se_3 thin film with diameters about 500 nm; the inset shows the flat surface of the ZnO NWs ($R_q = 33.3$ nm) which is beneficial for the deposition of Ag electrode. The rectifying characteristics of the current-voltage (*I–V*) curves presented in Fig. 1f indicate the formation of p-n junction; *I–V* curves of those 16 channels are demonstrated in Fig. S3b (Supporting Information), showing the good uniformity of the photodetector array. When the transmittance of the ITO glass is taken into consideration (Fig. S3d in the supporting information), it is obvious that the photoresponse of the device in the longer wavelength region outperforms the shorter wavelength region's at the same light intensity (25 mW/cm^2) for the output current increases gradually with the wavelength at a forward bias voltage of 1V. In other words, the photoresponse of the device shows a light wavelength dependence, which is significant for the realization of dual-polarity response.

As illustrated in Fig. 2a, the photoresponse performance of the self-powered PD under different wavelengths of light illumination with the same light intensity (25 mW/cm^2) was systematically investigated. *I-t* curves of the self-powered PD under periodical light illuminations show good stability and repeatability. Besides, the definition of forward connection (reversed connection) is when the ITO (Ag) and Ag (ITO) electrode is connected the positive and negative pole of the current meter, respectively. Under forward connection, as demonstrated in Fig. 2a (left half part), the photocurrent in the short (405 nm–690 nm) and long (760 nm–880 nm) wavelength region shows opposite polarity. However, it is well known that a positive photocurrent will be generated when such kind of p-n junction based PDs are at forward connection due to the photovoltaic effect. So it can be inferred that the output current in the longer wavelength region (760 nm–880 nm) is generated by the photovoltaic effect of the p-n junction. The negative output current in the shorter wavelength region (405 nm–690 nm) hints that PTE effect may play its part which will be discussed thoroughly later. To further confirm that the signals are from the device, the output signals under different wavelengths of light illumination were systematically measured when the device was at reversed connection to the measure system (right half part of Fig. 2a); reversed output signals are obtained which imply that previous signals are generated by the device.

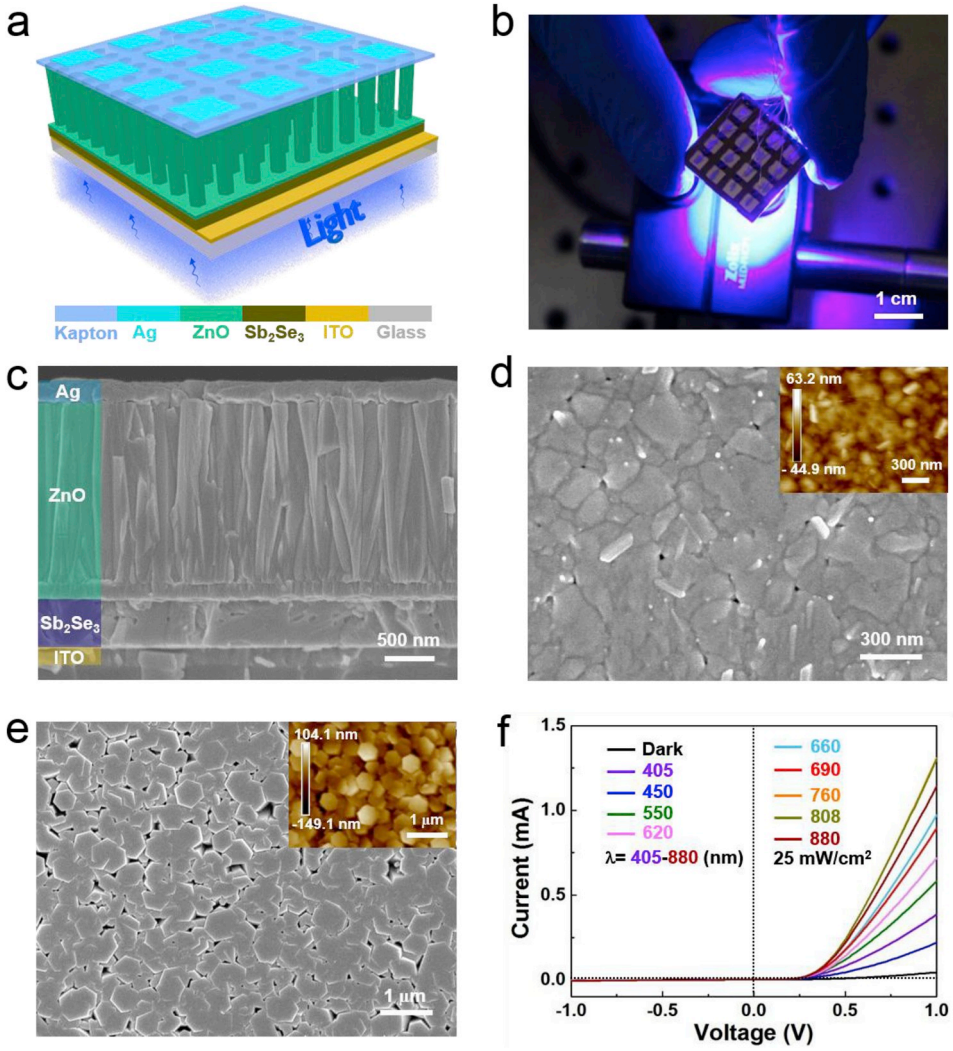

Fig. 1. Structure and *I–V* curves of the photodetector. (**a,b**) Schematic diagram (a) and optical image (b) of the ZnO NWs/Sb_2Se_3 heterojunction photodetector array. (**c**) Cross-sectional SEM image of the fabricated device. (**d,e**) SEM image of the annealed Sb_2Se_3 thin film (d) and ZnO NWs (e); the insets are the corresponding AFM images. (**f**) *I–V* characteristics of the photodetector under dark and different wavelengths of light illumination (25 mW/cm^2).

To better compare the output current under different wavelengths of light illumination, *I-t* curves in Fig. 2a (left half part) were normalized by light intensity and concisely illustrated in Fig. 2b. It can be easily seen that the polarity of the normalized current shows a dependence on light wavelength, where the current signals are negative when the wavelengths of the light illumination are shorter than or equal to 690 nm; however, when the wavelengths are longer or equal to 760 nm, the output current signals are positive. The output current signals demonstrated in Fig. 2a (left half part) are further summarized in Fig. 2c. The output current increases from about −8 nA to 69 nA, as the light wavelengths increase from 405 nm to 880 nm. Besides, between 690 nm and 760 nm may exist a polarity switching wavelength, where the current signal generated by the photovoltaic effect of p-n junction is exactly counteracted by PTE signal that is equal in magnitude but opposite in polarity. According to the photocurrent and corresponding light intensity, the responsivity (R) of the photodetector can be calculated out. The responsivity of self-powered PDs is defined as the following formula [7,36,37].

$$R = \frac{I_{ph} - I_d}{PS} \tag{1}$$

where I_{ph} is the photocurrent at a certain light intensity P, I_d is the corresponding dark current, and S denote the effective area of the device. As demonstrated in Fig. 2c the obtained responsivity was depicted as a function of light wavelength. The responsivity increase from about −3.7 μA/W to 30.6 μA/W, as the light wavelengths increase from 405 nm to 880 nm. Although the responsivity of the self-powered PD is relatively low in comparison with some existing self-powered PDs, the dual-polarity responsivity behavior make it totally different from those traditional self-powered PDs based p-n junction [3,6,33,38].

According to the responsivity and corresponding wavelength, the external quantum efficiency (EQE) of the photodetector can be obtained. The EQE of the self-powered PD is obtained according the following equation [7,36,37].

$$\mathrm{EQE} = \frac{hc}{q\lambda}R \tag{2}$$

where h is the Planck constant, c is the light speed, and λ denotes the light wavelength. As shown in Fig. S4b (Supporting Information), the EQE of the self-powered PD is displayed as a function of light wavelength. The EQE increase monotonically with light wavelength; more importantly, the negative EQE in the short wavelength region hints that this device is completely different from conventional photovoltaic device based on p-n junction [29–33].

As demonstrated in Fig. 3, the working mechanism of the dual-polarity response in the self-powered PD is revealed from the aspect of

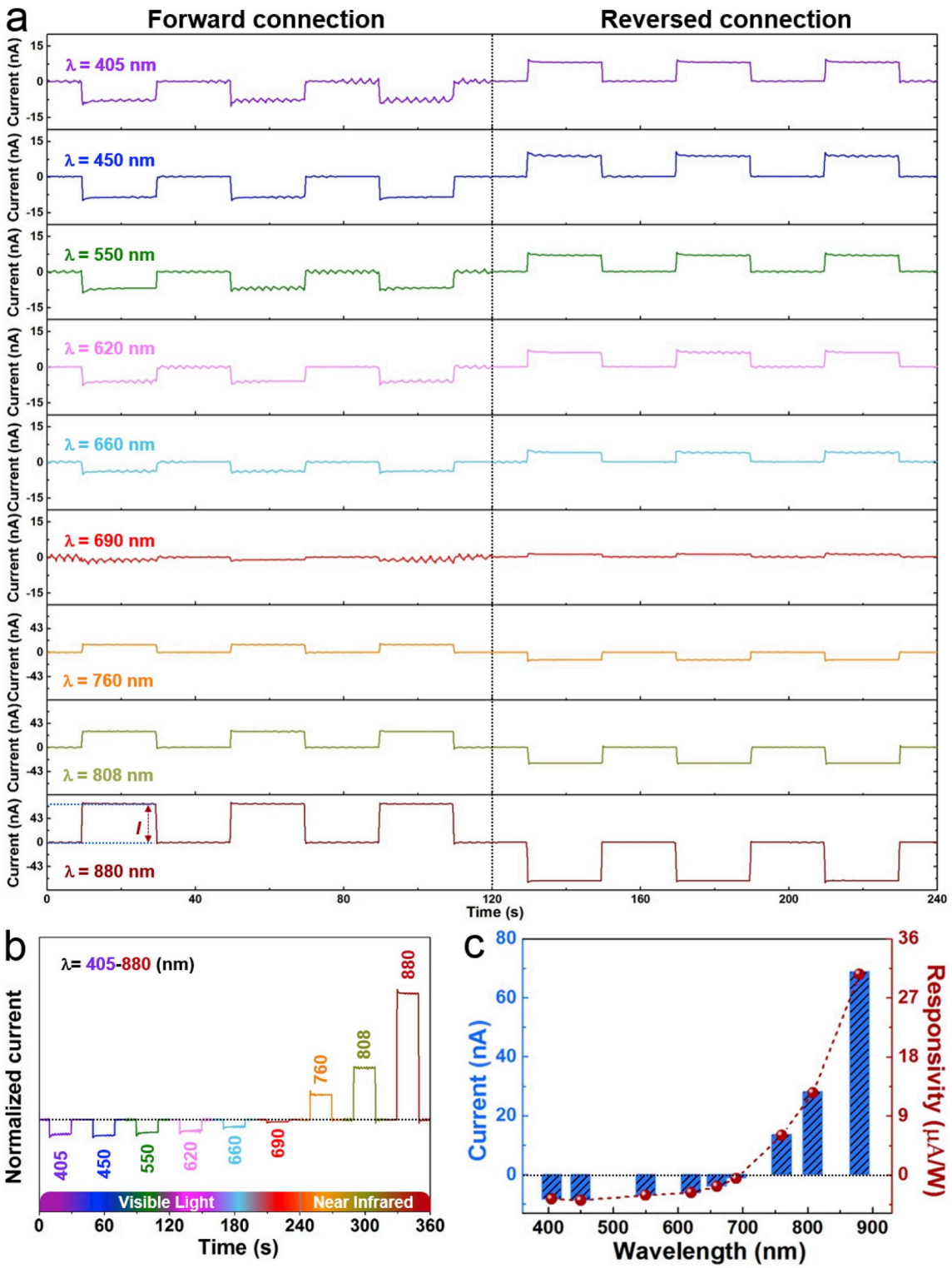

Fig. 2. Dual-polarity response performance of the photodetector. (**a**) *I-t* curves of the photodetector under different wavelengths of cyclic light illuminations (25 mW/cm^2) when it was at forward and reversed connection to the measure system. (**b**) Normalized photocurrent of the photodetector under different wavelengths of light illumination. (**c**) Output current extracted from **a** and corresponding responsivity as a function of wavelength.

energy band. The electron affinity and band gap of Sb_2Se_3 is 4.15 eV and 1.2 eV [33], respectively; for the ZnO, the electron affinity and band gap is 4.35 eV and 3.37 eV [39], respectively. Traditionally, the transparent wide band gap layer (ZnO) will be designed as the window layer, so the incident photons can successfully reach the interface of the p-n junction [24,29,30,39]. Then, under the excitation of incident photons, electron-hole pairs will be generated in the absorber material (Sb_2Se_3) near the interface of p-n junction. Subsequently, the electron-hole pairs will be effectively separated by the built-in electric field near the interface of p-n junction, and finally collected by the electrodes [24].

However, in this work, the absorber material (Sb_2Se_3) is used as the window layer (Fig. 3a,c). It is worth noticing that Sb_2Se_3 possess very

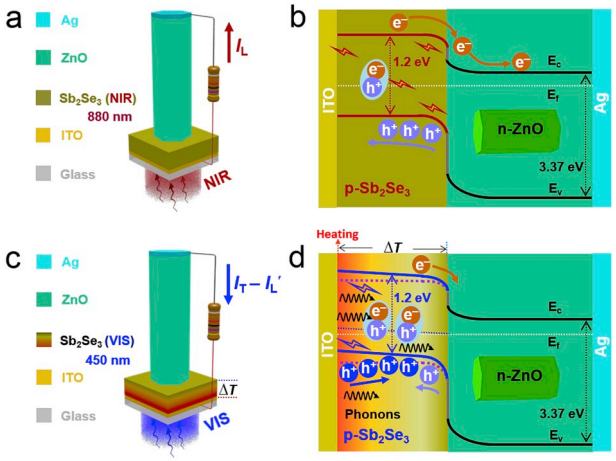

Fig. 3. Working mechanism of the photodetector. (**a,b**) Schematic working state (a) and energy band diagram (b) of the photodetector when it was under 880 nm light illumination. (**c,d**) Schematic working state (c) and energy band diagram (d) of the photodetector when it was under 880 nm light illumination.

high absorption coefficient, and the absorption coefficient (α) increases monotonically from about 0.7 × 10^5 cm^{-1} to 5.3 × 10^5 cm^{-1} as the photon energy increases from 1.4 eV (880 nm) to 2.8 eV (450 nm) [34]. Through the following equation we can estimate the absorption depth of the incident light, which is significant for the photovoltaic device based on p-n junction [27].

$$I_v(x) = I_{v0}e^{-\alpha x} \tag{3}$$

$$x = \frac{\ln[I_{v0}/I_v(x)]}{\alpha} \tag{4}$$

where I_v (x) is the light intensity at a certain penetration depth x, I_{v0} denotes the light intensity of the incident light, α represents the absorption coefficient. According to equation (3) and the absorption coefficient obtained from the references, for the 880 nm wavelength incident light, about 3% of the incident photons can penetrate the Sb_2Se_3 thin film (thickness: ~500 nm), which is in general agreement with the experiment data (Fig. S3d in the supporting information). Thus, the absorption depth can be properly estimated by equation (4). For 880 nm and 450 nm wavelength incident lights, 90% of the incident photons will be absorbed within a depth about 329 nm and 43 nm, respectively. Besides, since x is reversely proportional to α and α increases monotonically with photon energy, absorption depth decreases monotonically with photo energy. In other words, as the wavelength of the incident light increases from 405 nm to 880 nm, the absorption depth increases monotonically from about 43 nm to 329 nm. Thus, the longer wavelength will induce stronger photovoltaic effect for the incident photons can get closer to the interface of the p-n junction (the photo-generated electron-hole pairs can be more effectively separated by the built-in electric field). Experimentally, this inference can be confirmed by the EQE-wavelength curve in Fig. S4b (Supporting Information).

On the other hand, it is noteworthy that Sb_2Se_3 possess good thermoelectric performance, large Seebeck coefficient (~661 μV/K) had been found in Sb_2Se_3 nano materials [32,33]. Besides, Strong PTE effect had been confirmed in MoS_2 and graphene nano flakes, where the PTE current can be attributed the temperature gradient caused by the local illumination of the laser and the large Seebeck coefficient of the material [26,27]. Moreover, the output current of the nano device shows an illumination position-dependence (the output current increases monotonically as the laser spot swept from one end to the middle of the device). In this work, since 90% of the incident photons (450 nm) will be absorbed within a depth about 43 nm, a considerable temperature gradient may be established across the Sb_2Se_3 thin film (~500 nm in thickness). As displayed in Fig. S5 (Supporting Information), the surface temperature of the device rises about 2 K under light illumination. According to the above analysis, the PTE effect should be taken into consideration in this device. The PTE effect was experimentally confirmed by an ITO/Sb_2Se_3/ITO ohmic-junction device with an effect area of 3 mm × 3 mm (Figure S6a,b and S7a,b in the supporting information). Negative output signals are observed when the glass side of the device is under 450 nm light illumination (Figs. S6c and e in the supporting information); the polarity of the PTE current is the same as the polarity of the current demonstrated in Fig. 2a (450 nm). The PTE effect is further confirmed by changing the light direction. As illustrated in Figs. S7c and e (Supporting Information) positive output signals are obtained when the opposite side of the device is under 450 nm light illumination (reversed temperature gradient will be induced by the light illumination). In addition, the shorter wavelength will induce stronger PTE effect, for the absorption depth of the incident light decreases monotonically as the wavelength varies from 880 nm to 450 nm. This inference can be experimentally confirmed by the EQE-wavelength curve in Fig. S4b (Supporting Information).

In the long wavelength region (760 nm–880 nm), the output current flow from ITO electrode to Ag electrode in the external circuit (Fig. 3a), which can be mainly attributed to the PV effect of the p-n junction (Fig. 3b). In the short wavelength region (405 nm–690 nm), the output currents flow from Ag electrode to ITO electrode (Fig. 3c), which can be mainly attributed to the PTE effect of the Sb_2Se_3 thin film (Fig. 3d). Apparently, the dual-polarity response in the self-powered PD is a consequence of the competition between PV effect and PTE effect. In the long wave length region, the PV effect outperforms the PTE effect; in the short wavelength region, the PTE effect outperforms the PV effect. A polarity switching wavelength exists between 690 nm and 760 nm, where the PV effect and PTE effect cancel each other. Most importantly, the polarity switching wavelength can be accurately controlled by modulating the efficiency of the PV effect and PTE effect. For instance, increasing (decreasing) the thickness of Sb_2Se_3 thin film will shift the polarity switching point to a shorter (longer) wavelength. Moreover, the polarity switching point can also be modulated by the absorption coefficient, carrier concentration, thermal conductivity, Seebeck coefficient, band gap, barrier height at the interface, and so on.

The photodetection performance of the self-powered PD under 450 nm and 880 nm wavelengths light illumination was systematically investigated and illustrated in Fig. 4. As illustrated in Fig. 4a, the output current under cyclic light illumination exhibits good stability and repeatability. Besides, under 450 nm wavelength light illumination (140 mW/cm^2), the output current is about −21.1 nA; under 880 nm wavelength light illumination (25 mW/cm^2), the output current is about 25.3 nA. *I*-t curves of the self-powered PD under 450 nm and 880 nm wavelengths light illumination with different light intensities are shown in Fig. 4b. To better demonstrate the variation trend of the output current, the information in Fig. 4b is further summarized in Fig. 4c and d. The output current is about −3.8 nA under 450 nm wavelength light illumination with a light intensity of 14 mW/cm^2 and the absolute value of the output current increases monotonically when the light intensity increases from to 14 mW/cm^2 to 140 mW/cm^2 (Fig. 4c). The corresponding responsivity is also demonstrated in Fig. 4c, a maximum responsivity (−3.5 μA/W) is obtained at a light intensity of 14 mW/cm^2 and the absolute value of the responsivity shows a decreasing trend as the light intensity increases. As displayed in Fig. 4d, the output current is about 14.9 nA under 880 nm wavelength light illumination with a light intensity of 7 mW/cm^2. Besides, the output current increases monotonically with light intensity. The corresponding responsivity shows a decreasing trend when the light intensity increases from 4 mW/cm^2 to 25 mW/cm^2; a maximum responsivity of 40.8 μA/W is obtained at a light intensity of 4 mW/cm^2. Though the responsivity of the self-powered PD is relatively low, it can be largely improved by optimizing the Sb_2Se_3 thin film [31]. In addition, the polarity of the output current under different light intensities remains unchanged, which

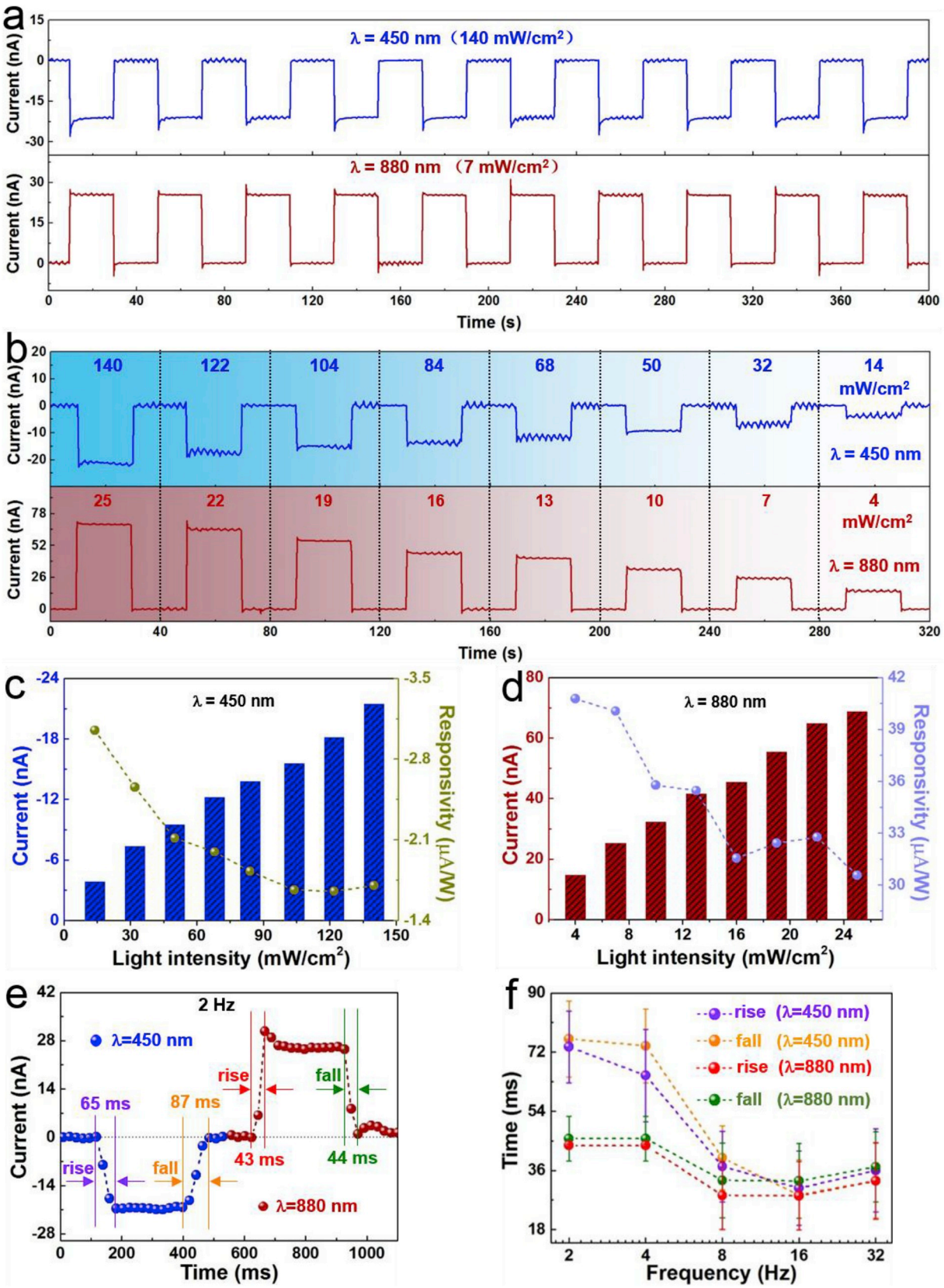

Fig. 4. General performance of the photodetector. (**a**) *I-t* curves of the photodetector under periodical 450 nm (140 mW/cm^2) and 880 nm (25 mW/cm^2) wavelength light illumination. (**b**) *I-t* curves of the photodetector under 450 nm and 880 nm wavelength light illumination with different light intensities. (**c, d**) Output current extracted from **b** and corresponding responsivity as a function of light intensity. (**e**) Responsivity of the photodetector under 405 nm and 880 nm wavelength light illumination. (**f**) Response speed of the photodetector as a function of the frequency optical chopper.

imply that the polarity is independent of light intensity (Fig. 4c and d). The corresponding temperature information under different light intensities can be found in Fig. S8 (Supporting Information).

To character the response speed of the self-powered PD under 450 nm and 880 nm light illuminations, a commercial optical chopper was used to produce cyclic light illuminations. *I*-t curves of the self-powered PD under different on-off frequencies are shown in Fig. S10b (Supporting Information). To better illustrate the response speed of the self-powered PD, part of the *I*-t curves are enlarged and shown in Fig. 4e (chopper frequency: 2 Hz). Under 450 nm wavelength light illumination (140 mW/cm^2), the rise and fall time is shorter than 65 ms and 87 ms, respectively. The self-powered PD exhibits a faster response speed under 880 nm wavelength illumination (7 mW/cm^2), the rise and fall time is shorter than 43 ms and 44 ms, respectively. The response speed of the self-powered PD was further investigated by varying the frequency of the optical chopper from 2 Hz to 32 Hz. As depicted in Fig. 4f, the rise and fall time of the self-powered PD shows a decreasing trend. At a frequency of 16 Hz, the average rise and fall time is shorter than 29 ms and 31 ms for 450 nm wavelength light illumination; for 880 nm wavelength light illumination, the average rise and fall time is shorter than 33 ms and 28 ms, respectively. Due to the limitation of the measure system, the actual response speed of the self-powered PD could even be faster.

To better demonstrate the application prospect of the dual-polarity response PD, a prototype of bipolar CSK system diagram is shown in Fig. 5c. Unipolar or bipolar code can be transferred to LEDs through a lighting controller. When 880 (450) nm wavelength LED is activated, positive (negative) signal is modulated on the light. Then, the data

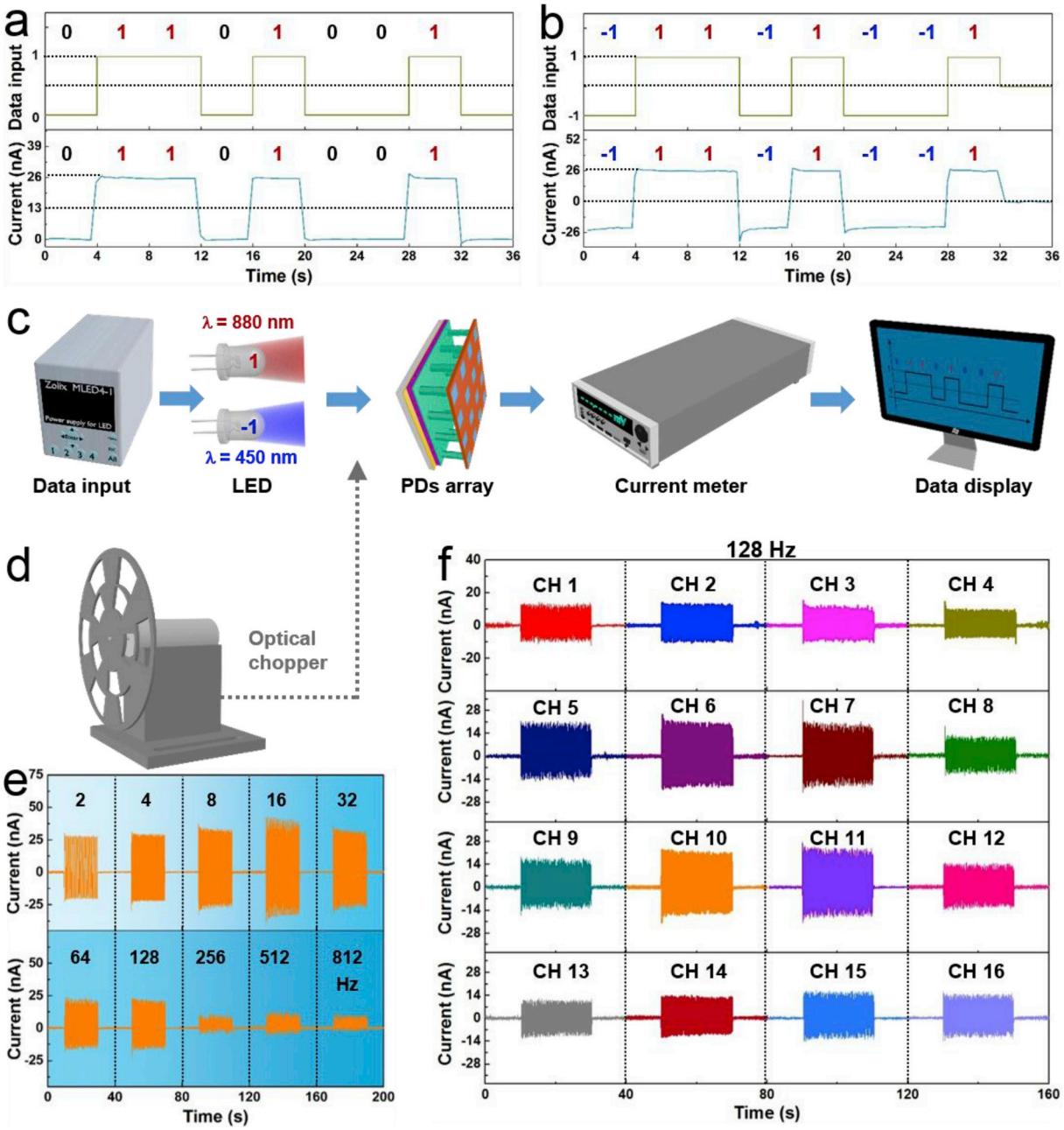

Fig. 5. Optical communication application based on the dual-polarity response photodetector. (**a**) The waveform of an unipolar input signal and the signal received by the photodetector. (**b**) The waveform of an bipolar input signal and the signal received by the photodetector. (**c**,**d**) Schematic diagram of the optical communication system. (**e**) Bipolar signals received by the photodetector at different transmitted rates. (**f**) Bipolar signals received by the photodetector array at a certain transmitted rate.

modulated on the light will be recovered by the receiver (PD) and finally displayed on a computer. As illustrated in Fig. 5a, unipolar code can be successfully transmitted through the 880 nm wavelength LED and recovered by the receiver (traditional on-off keying modulation), for the waveform of the photocurrent is the same as the input data. Most importantly, as displayed in Fig. 5b, bipolar code from 450 nm to 880 nm wavelength LEDs can be successfully recovered by only one pixel without the help of any filter (CSK modulation). To reveal the transmission rate of the CSK system, a commercial optical chopper was used to enable the receiver alternately illuminated by 450 nm and 880 nm wavelength LEDs, which means that data bits "1"and "-1" are alternately transmitted (Fig. 5d). As illustrated in Fig. 5e, a maximum transmission rate about 18 bps is obtained as the frequency of the optical chopper is adjusted to 128 Hz. Due to the limitation of the current meter, the bit rate could even be far higher than the experiment data. The application of the photodetector array (4 × 4) is demonstrated in Fig. 5f, each pixel can receive data from LEDs at bit rate about 18 bps, which may be useful for accurate indoor positioning in VLC system [16].

4. Conclusion

In summary, we have designed a new type of dual-polarity response self-powered photodetector based on ZnO NWs/Sb_2Se_3 heterojunction, where the polarity of the output signal can be controlled by the light wavelength. The dual-polarity response is associated with the competition between the PTE effect in Sb_2Se_3 thin film and the PV effect of ZnO NWs/Sb_2Se_3 p-n junction. As the wavelength increases from 405 to 880 nm, the PV effect will get stronger while the PTE effect get weaker. As a result, the output signals are positive in the long wavelength region (760–880 nm) for the PV effect outperforms the PTE effect; in the short wavelength region (405–690 nm), the output signals are negative for the PTE effect outperforms the PV effect. Moreover, the self-powered PD possesses a fast response speed, under 450 nm wavelength light illumination the average rise and fall time is shorter than 29 and 31 ms; for 880 nm wavelength light illumination, the average rise and fall time is shorter than 33 and 28 ms. Finally, the dual-polarity response self-powered PD was successfully used as a receiver in a bipolar CSK system and the application of the photodetector array (4 × 4) exhibits potential in accurate indoor positioning. As compared with current receivers in CSK systems, our receiver can work without any filter and one receiver can realize the function of two traditional receivers [17]. Our PD can reduce the costs of device fabrication and simply the communication system, exhibiting a great application potential in VLC system. Further improvements of the dual-polarity PD can be envisioned by optimizing the absorber material or introducing more appropriate n-type material to boost the responsivity [31].

Declaration of competing interest

The authors declare that they have no known competing financial interests or personal relationships that could have appeared to influence the work reported in this paper.

Acknowledgments

This work was supported by the National Key R&D Program of China (Grant No. 2016YFA0202701), National Natural Science Foundation of China (Grant No. 51472055), External Cooperation Program of BIC, Chinese Academy of Sciences (Grant No. 121411KYS820150028), the 2015 Annual Beijing Talents Fund (Grant No. 20150000021223ZK32), Qingdao National Laboratory for Marine Science and Technology (No. 2017ASKJ01), and the University of Chinese Academy of Sciences (Grant No.Y8540XX2D2).

Appendix A. Supplementary data

Supplementary data to this article can be found online at https://doi.org/10.1016/j.nanoen.2019.104312.

References

[1] J. Clark, G. Lanzani, Nat. Photonics 4 (2010) 438–446.
[2] Q. Lin, A. Armin, P.L. Burn, P. Meredith, Nat. Photonics 9 (2015) 687–694.
[3] X. Lu, P. Jiang, X. Bao, Nat. Commun. 10 (2019) 138.
[4] H. Fang, C. Zheng, L. Wu, Y. Li, J. Cai, M. Hu, X. Fang, R. Ma, Q. Wang, H. Wang, Adv. Funct. Mater. 29 (2019) 1809013.
[5] B. Ouyang, K. Zhang, Y. Yang, Adv. Mater. Technol. 2 (2017) 1700208.
[6] Y. Dai, X. Wang, W. Peng, C. Xu, C. Wu, K. Dong, R. Liu, Z.L. Wang, Adv. Mater. 30 (2018) 1705893.
[7] Z. Wang, R. Yu, C. Pan, Z. Li, J. Yang, F. Yi, Z.L. Wang, Nat. Commun. 6 (2015) 8401.
[8] C. Bao, J. Yang, S. Bai, W. Xu, Z. Yan, Q. Xu, J. Liu, W. Zhang, F. Gao, Adv. Mater. 30 (2018) 1803422.
[9] H. Zhang, X. Zhang, C. Liu, S.T. Lee, J. Jie, ACS Nano 10 (2016) 5113–5122.
[10] D. Guo, Y. Su, H. Shi, P. Li, N. Zhao, J. Ye, S. Wang, A. Liu, Z. Chen, C. Li, W. Tang, ACS Nano 12 (2018) 12827–12835.
[11] S.F. Leung, K.T. Ho, P.K. Kung, V.K.S. Hsiao, H.N. Alshareef, Z.L. Wang, J.H. He, Adv. Mater. 30 (2018) 1704611.
[12] H. Sun, W. Tian, F. Cao, J. Xiong, L. Li, Adv. Mater. 30 (2018) 1706986.
[13] X.J. Xu, J.X. Chen, S. Cai, Z.H. Long, Y. Zhang, L.X. Su, S.S. He, C.Q. Tang, P. Liu, H.S. Peng, X.S. Fang, Adv. Mater. 30 (2018) 1803165.
[14] P.H. Pathak, X. Feng, P. Hu, P. Mohapatra, IEEE Commun. Surv. Tutor. 17 (2015) 2047–2077.
[15] T. Komine, J.H. Lee, S. Haruyama, M. Nakagawa, IEEE Trans. Wirel. Commun. 8 (2009) 2892–2900.
[16] A. Jovicic, J. Li, T. Richardson, IEEE Commun. Mag. 51 (2013) 26–32.
[17] W. Xu, H. Shen, J. Wang, H. Zhang, Electron. Lett. 52 (2016) 133–135.
[18] N. Murata, Y. Kozawa, Y. Umeda, IEEE Photonics J. 8 (2016) 1–13.
[19] L.X. Liang, M. Yuan, J. Wang, Z. Ding, M. Jiang, C. Zhao, J. Light. Technol. 35 (2017) 3650–3663.
[20] Y.Q. Bie, Z.M. Liao, H.Z. Zhang, G.R. Li, Y. Ye, Y.B. Zhou, J. Xu, Z.X. Qin, L. Dai, D. P. Yu, Adv. Mater. 23 (2011) 649–653.
[21] X. Cai, A.B. Sushkov, R.J. Suess, M.M. Jadidi, G.S. Jenkins, L.O. Nyakiti, R. L. Myers-Ward, S. Li, J. Yan, D.K. Gaskill, T.E. Murphy, H.D. Drew, M.S. Fuhrer, Nat. Nanotechnol. 9 (2014) 814–819.
[22] L.Y.S. Lai, C.Y. Tsai, C.K. Chang, C.Y. Huang, V.K. Hsiao, Y.O. Su, Adv. Mater. 28 (2016) 2644–2648.
[23] X. He, X. Wang, S. Nanot, K. Cong, Q. Jiang, A.A. Kane, J.E. Goldsmith, R. H. Hauge, F. Leonard, J. Kono, ACS Nano 7 (2013) 7271–7277.
[24] A.J. Heeger, Adv. Mater. 26 (2014) 10–27.
[25] W. Ouyang, F. Teng, J.-H. He, X. Fang, Adv. Funct. Mater. 29 (2019) 1807672.
[26] N.M. Gabor, J.C.W. Song, Q. Ma, N.L. Nair, T. Taychatanapat, K. Watanabe, T. Taniguchi, L.S. Levitov, P. Jarillo-Herrero, Science 334 (2011) 648–652.
[27] M. Buscema, M. Barkelid, V. Zwiller, H.S. van der Zant, G.A. Steele, A. Castellanos-Gomez, Nano Lett. 13 (2013) 358–363.
[28] J.C. Song, M.S. Rudner, C.M. Marcus, L.S. Levitov, Nano Lett. 11 (2011) 4688–4692.
[29] Y. Zhou, L. Wang, S. Chen, S. Qin, X. Liu, J. Chen, D.-J. Xue, M. Luo, Y. Cao, Y. Cheng, E.H. Sargent, J. Tang, Nat. Photonics 9 (2015) 409–415.
[30] L. Wang, D.-B. Li, K. Li, C. Chen, H.-X. Deng, L. Gao, Y. Zhao, F. Jiang, L. Li, F. Huang, Y. He, H. Song, G. Niu, J. Tang, Nat. Energy 2 (2017) 17046.
[31] X. Wen, C. Chen, S. Lu, K. Li, R. Kondrotas, Y. Zhao, W. Chen, L. Gao, C. Wang, J. Zhang, G. Niu, J. Tang, Nat. Commun. 9 (2018) 2179.
[32] K.T.Y. Ko, M. Shellaiah, K.W. Sun, Sci. Rep. 6 (2016) 35086.
[33] X. Liu, J. Chen, M. Luo, M. Leng, Z. Xia, Y. Zhou, S. Qin, D.J. Xue, L. Lv, H. Huang, D. Niu, J. Tang, ACS Appl. Mater. Interfaces 6 (2014) 10687–10695.
[34] M. Kamruzzaman, C. Liu, A.K.M. Farid Ul Islam, J.A. Zapien, Semiconductors 51 (2017) 1615–1624.
[35] J. Li, J. Wang, J. Ma, H. Shen, L. Li, X. Duan, D. Li, Nat. Commun. 10 (2019) 806.
[36] F. Teng, K. Hu, W.X. Ouyang, X.S. Fang, Adv. Mater. 30 (2018) 39.
[37] X. Liu, L. Gu, Q. Zhang, J. Wu, Y. Long, Z. Fan, Nat. Commun. 5 (2014) 4007.
[38] L. Zhang, Y. Li, C. Li, Q. Chen, Z. Zhen, X. Jiang, M. Zhong, F. Zhang, H. Zhu, ACS Nano 11 (2017) 12753–12763.
[39] H. Zou, X. Li, W. Peng, W. Wu, R. Yu, C. Wu, W. Ding, F. Hu, R. Liu, Y. Zi, Z. L. Wang, Adv. Mater. 29 (2017) 1701412.

Bangsen Ouyang is a Ph.D student in the research group of Professor Ya Yang at Beijing Institute of Nanoenergy and Nanosystems, Chinese Academy of Sciences (CAS). He received his bachelor's degree in Applied Physics from Xihua University in 2014. His current interests focus on self-powered photodetector.

Huiqi Zhao is a graduate student in the research group of Professor Ya Yang at Beijing Institute of Nanoenergy and Nanosystems, CAS. Her main research interests focus on the field of self-powered systems, photoelectric sensor and piezoelectric materials.

Prof. Zhong Lin (ZL) Wang received his Ph.D. from Arizona State University in physics. He now is the Hightower Chair in Materials Science and Engineering, Regents' Professor, Engineering Distinguished Professor and Director, Center for Nanostructure Characterization, at Georgia Tech. Dr. Wang has made original and innovative contributions to the synthesis, discovery, characterization and understanding of fundamental physical properties of oxide nanobelts and nanowires, as well as applications of nanowires in energy sciences, electronics, optoelectronics and biological science. His discovery and breakthroughs in developing nanogenerators established the principle and technological road map for harvesting mechanical energy from environment and biological systems for powering a personal electronics. His research on self-powered nanosystems has inspired the worldwide effort in academia and industry for studying energy for micro-nano-systems, which is now a distinct disciplinary in energy research and future sensor networks. He coined and pioneered the field of piezotronics and piezophototronics by introducing piezoelectric potential gated charge transport process in fabricating new electronic and optoelectronic devices. Details can be found at: http://www.nanoscience.gatech.edu.

Prof. Ya Yang received his Ph.D in Materials Science and Engineering from University of Science and Technology Beijing, China. He is currently a professor at Beijing Institute of Nanoenergy and Nanosystems, CAS. His main research interests focus on the field of pyroelectric, piezoelectric, triboelectric, and thermoelectric nanogenerators for energy conversion, storage and some novel applications.